

Normal state of metal-intercalated phenacene crystals: Role of electron correlations

Tirthankar Dutta¹ and Sumit Mazumdar¹

¹*Department of Physics, University of Arizona, Tucson, AZ 85721*

(Dated: July 13, 2016)

In this work we study the effect of long range electron-electron correlations on the behavior of the normal state of metal-intercalated phenacene crystals. While the individual phenacene molecules are modeled by the Pariser-Parr-Pople Hamiltonian with long range Coulomb interactions, we derive a correlated minimal model for describing the phenacene ionic crystals. We find that long range electron correlations do not change the behavior of the phenacene ions with molecular valence -1 (monoanion) and -2 (dianion), compared to that observed for short range electron interactions. The monoanion crystal is a single-band $\frac{1}{2}$ -filled antiferromagnetic Mott-Hubbard semiconductor while the dianion crystal is a two-band semiconductor with inter-molecular antiferromagnetic and intra-molecular ferromagnetic spin orderings. However, the trianion crystal is no longer a nearly degenerate $\frac{3}{4}$ -filled two-band system. We show that this occurs because the kinetic stability of the $\frac{3}{4}$ -filled two-band system with long range correlations is smaller compared to that with short range correlations, for the lattice sizes considered in this study. We argue that with large finite lattices, behavior of the trianion crystal with long range correlations will be same as that with short range correlations. We thus conclude that long range correlations fail to alter the normal states of metal-intercalated phenacene crystals.

PACS numbers: 71.10.Fd, 74.20.Mn, 74.70.Kn, 74.70.Wz

I. INTRODUCTION

Strongly correlated multi-orbital systems lie at the forefront of modern day condensed matter physics. Interaction between the charge, spin and orbital degrees of freedom of the electrons in these systems leads to various novel phenomena like, giant magnetoresistance, itinerant ferromagnetism, charge-orbital ordering, and superconductivity (SC)¹⁻⁸. Among the multi-orbital superconductors, many show SC at a fixed or very narrow region of carrier density. The ones which are of particular interest to us are the carbon(C)-based unconventional superconductors such as the charge-transfer solids (CTS)⁹, alkali metal-doped fullerides (A_3C_{60})¹⁰⁻¹², and the metal-intercalated phenacenes¹³⁻¹⁹. Experimentally it is found that SC in the CTS occur under pressure and at the carrier density $\rho \approx 0.5$ ^{20,21}; ρ is defined as the ratio of the number of charge carriers to the number of active orbitals, i.e., $N_{e(h)}/N_o$, where $e(h)$ refer to electron(hole). Similarly, doped fullerides and metal-intercalated phenacenes are found to show SC under pressure and at molecular valence -3 , which correspond to $\rho = 1.5$ ²²; note that $\rho = 1.5$ (electrons as charge carriers) and $\rho = 0.5$ (holes as charge carriers) are equivalent. Three different classes of C-based materials showing SC at a fixed carrier concentration raises an important question: Is there something special about carrier density 0.5?

In order to understand the mechanism of SC in these multi-orbital C-based systems it is important to first understand the normal state at this particular carrier concentration. It is with this motivation that we began the investigation of the electronic structure of metal-doped phenacenes²², which have been claimed to be superconducting¹³⁻¹⁹ only at molecular valence -3 . After the discovery of SC in metal-intercalated phenacenes,

other groups have failed to reproduce the results obtained by Kubozono *et. al.* for picene^{13,14} and Wang *et. al.* for phenanthrene¹⁵⁻¹⁷. However recently, Artioli *et. al.* have reported SC in Sm-doped phenanthrene, chrysene, and picene²³. They conclude that the presence of SC at molecular valence -3 irrespective of the number of phenacene rings “raises new questions that open the way for further and new theoretical investigations on the electron pairing mechanism” in polycyclic aromatic hydrocarbons.

In addition to the work of Artioli *et. al.*, we believe that a proper theoretical understanding of the normal state of metal-intercalated phenacenes (phenanthrene and picene) is of interest from another perspective, namely, understanding pressure-induced antiferromagnetic-to-SC transition in $A15$ Cs_3C_{60} ^{24,25}. In what follows, the terms monoanion, dianion and trianion will refer to M^{1-} , M^{2-} and M^{3-} , respectively; here, M refer to a molecule and the superscript denote the charge of M , i.e., number of doped electrons. In both phenacenes and fullerides (for which experimental results are robust), there is apparent breaking of charge conjugation symmetry, i.e., crystals of monocations and trianions behave differently. While molecular solids of phenacene and fulleride trianions show SC, crystals of their monoanions are semiconducting. In neutral C_{60} molecules, the Lowest Unoccupied Molecular Orbitals (LUMOs) are empty and triply degenerate; the levels are referred to as t_{1u} . Upon electron doping, by virtue of Jahn-Teller distortion and electron-electron (e-e) interactions, this degeneracy is lifted; for illustration sake we shall denote these non-degenerate levels as t_{1u}^n , where the superscript n refer to the orbital occupancy. Thus, each C_{60}^{3-} ion consists of a low lying t_{1u}^2 orbital, a t_{1u}^1 orbital at intermediate energy, and a high lying t_{1u}^0 or-

bital. Similarly, each C_{60}^{1-} ion have a low lying t_{1u}^1 orbital and two degenerate t_{1u}^0 orbitals. It is widely believed that the ambient pressure antiferromagnetism in C_{60}^{3-} crystals arise from inter-molecular spin-spin coupling between electrons occupying the t_{1u}^1 orbitals. This $\frac{1}{2}$ -filled Mott insulator under pressure becomes superconducting due to increased band-width^{12,26–28}. This viewpoint of SC in the fullerenes however has some drawbacks. Firstly, this theory is based on the results of mean field and dynamical mean field theory (DMFT) studies showing antiferromagnetic-to-SC transition in the frustrated $\frac{1}{2}$ -filled Hubbard model^{29–33}. However, more recent and sophisticated numerical calculations which go beyond mean field level have shown the absence of SC in the frustrated $\frac{1}{2}$ -filled Hubbard model^{34–39}. Secondly, this approach fails to explain the absence of SC in fulleride monoanion crystals which are also $\frac{1}{2}$ -filled antiferromagnetic Mott insulators; the t_{1u}^1 orbitals of C_6^{1-} ions can couple antiferromagnetically in the solid state. Lastly, the absence of SC in the Mott-Hubbard semiconductor K₁pentacene⁴⁰ confirms the theories that predict absence of SC within the $\frac{1}{2}$ -filled band Hubbard model. Thus, a proper understanding of the normal state and hence the mechanism of SC in the fullerenes is still not complete.

In our previous study on phenanthenes²² we have shown that breaking of charge conjugation symmetry is a band-width induced effect, that gets further enhanced by electron correlations. A similar scenario is expected to hold for doped fullerenes also, thereby leading to an alternative description of SC in doped fullerenes within our theory of metal-intercalated phenanthenes. At ambient pressure molecular solids of both C_{60}^{1-} and C_{60}^{3-} are $\rho = 1$ antiferromagnetic Mott insulators. Under pressure there is equalization of electron population between the t_{1u}^2 and t_{1u}^1 levels of the trianions by virtue of inter-ion inter-orbital hoppings leading to the formation of a $\rho = 3/2$ two-band paramagnetic system. SC in this case will be related to populations of $3/2$ in two non-degenerate levels which become close in energy by virtue of increased band-width, and the pairing is inter-molecular rather than intra-molecular. Such a band-width induced population exchange will not occur in the monoanion crystal by virtue of its molecular charge and it continues to be a $\rho = 1$ antiferromagnet (AFM). We are unaware of any experiment in this context that would preclude our proposed mechanism.

In our previous work²², we have explicitly shown that in the presence of short range e-e interactions, the normal states of the monoanion and trianion crystals are not identical but differs substantially. These different normal states under pressure would have different behaviors and thus, while the monoanion crystal is an AFM, the trianion solid shows SC. A summary of our previous results is presented in Sec-III. The motivation behind the present study is to understand the effect of long range e-e interactions on the normal states of the phenacene ionic crystals. Our modeling of charged phenacene crys-

tals begins from an atomistic description of the individual molecules, described within a π -electron model. We construct localized molecular orbitals (MOs) for the individual phenacene molecules from which the description of the crystal is built using the frontier MOs (FMOs) as basis orbitals. Previously we had addressed the normal state of metal-intercalated phenanthenes by deriving an effective low-energy Hamiltonian, $H_{L,L+1}^{Hub}$, within the localized basis of the LUMO (L) and LUMO+1 (L+1) FMOs²², and describing the individual phenacene molecules by the Hubbard model having only on-site (short range) e-e correlations. But C-based materials like the phenanthenes are known to possess long range Coulomb correlations and thus, the Hubbard model is inadequate for their complete description. In the present work we model the individual phenacene molecules by the Pariser-Parr-Pople Hamiltonian (PPP)^{41,42} having true long range e-e interactions. The effective crystal Hamiltonian in this case is depicted by $H_{L,L+1}^{PPP}$. We find that long range interactions, apart from renormalizing the individual terms in $H_{L,L+1}^{Hub}$, introduce an additional repulsion term between *same spin* electrons occupying different orbitals on the same molecule (see Sec-II). We thus anticipate that long range correlations will not affect the normal state of the monoanion crystal but should alter the behavior of the dianion and trianion crystals. We find that long range e-e interactions only alter the behavior of the trianion crystal, although the monoanion-trianion asymmetry *persists*. We will show in Sec-IV that the change in behavior of the trianion crystal is due to the size of the lattices that we have considered. These small system sizes fail to provide the kinetic stability needed by the trianion crystal to behave as a nearly degenerate two-band $\frac{3}{4}$ -filled system (see Sec-III).

II. THEORETICAL MODELING AND COMPUTATIONAL DETAILS

Metal-intercalated phenanthenes crystallize in the Herringbone motif which is shown in Fig. 1. The complete Hamiltonian for such a solid can be written as $H = H_{intra} + H_{inter}$, where H_{intra} depict the intra-molecular Hamiltonian of individual phenacene molecules and H_{inter} represent the inter-molecular interactions. The intra-molecular Hamiltonian can be expressed as,

$$H_{intra} = -\epsilon \sum_{\mu,i}' n_{\mu,i} - t \sum_{\mu,\langle ij \rangle,\sigma} c_{\mu,i,\sigma}^\dagger c_{\mu,j,\sigma} + U \sum_{\mu,i} n_{\mu,i,\uparrow} n_{\mu,i,\downarrow} + \frac{1}{2} \sum_{\mu,i \neq j} V_{i,j} n_{\mu,i} n_{\mu,j} \quad (1)$$

In the above $c_{\mu,i,\sigma}^\dagger$ creates a π -electron of spin σ in the p_z orbital of the i -th *C-atom* of the μ -th molecular ion, $n_{\mu,i,\sigma} = c_{\mu,i,\sigma}^\dagger c_{\mu,i,\sigma}$, and $n_{\mu,i} = \sum_{\sigma} n_{\mu,i,\sigma}$. The primed sum in the site-energy dependent term of Eq. 1 is restricted to C-atoms without C-H bonds, accounting

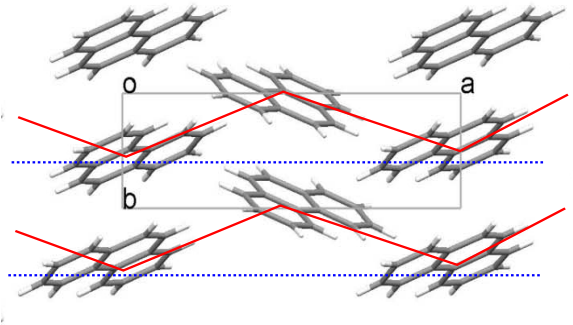


FIG. 1: (Color online) 2D Herringbone lattice of phenanthrene ions (the crystallographic motif is taken from Ref. 43); metal ions are not shown for clarity. The 1D lattice studied in text is shown superimposed on the 2D lattice by solid red and blue dashed lines, depicting nearest neighbor and next-nearest neighbor hoppings, respectively.

for their higher electronegativity than those with C-H bonds⁴⁴. The nearest neighbor ($\langle ij \rangle$) hopping integral of individual phenacene molecules is t ; we take $t = 2.4$ eV, which is the standard intra-molecular hopping integral for C-based systems. U represents the onsite Coulomb repulsion between two electrons of opposite spins occupying the $2p_z$ orbital of a C-atom of a phenacene molecule; we vary U from 0 – 10 eV in this study. The parametrized expression for the $V_{i,j}$ term, which depicts the intersite repulsion between two electrons on C-atoms i and j of a phenacene molecule, is given below.

$$V_{i,j} = \frac{U}{\kappa(1 + 0.6117R_{i,j}^2)^{1/2}}. \quad (2)$$

Here, $R_{i,j}$ (in Å) is the distance between C-atoms i and j of a phenacene molecule. The constant κ models the dielectric constant of the medium and determines the strength of $V_{i,j}$ as a function of distance⁴⁵. The above parametrization with $U = 11.13$ eV and $\kappa = 1$ corresponds to the Ohno parametrization⁴⁶.

The inter-molecular Hamiltonian can include hopping of electrons between the molecules (H_{inter}^{1e}), e-e repulsion between the charged phenacene ions (H_{inter}^{ee}), interactions between the metal ions and the molecules ($H_{inter}^{ion-mol}$), and interactions between the metal ions ($H_{inter}^{ion-ion}$). In this study we have neglected all the terms in H_{inter} except H_{inter}^{1e} , as they do not affect our generic qualitative theoretical model. These terms can be included later for deriving a quantitative theory. In what

follows,

$$H_{inter}^{1e} = \sum_{i \in \mu, j \in \nu, \sigma} t_{\mu, \nu, i, j} c_{\mu, i, \sigma}^\dagger c_{\nu, j, \sigma}. \quad (3)$$

Here, $t_{\mu, \nu, i, j}$ are the inter-molecular hopping integrals between C-atoms i and j of molecules μ and ν , respectively. Compared to the intra-molecular hopping term $t = 2.4$ eV, the inter-molecular hoppings are tiny and generally of the order of 0.1 – 0.2 eV (cf. 22).

Solving H in the complete space of $2p_z$ atomic orbitals is computationally impossible due to its overwhelmingly large dimension. We therefore work within the standard approach of molecular exciton theory and first transform H from the $2p_z$ atomic orbital basis to the MO basis; this unitary basis transform is exact. We then identify the FMOs for the problem and derive an effective Hamiltonian in the reduced subspace of the FMOs. In the case of phenacenes, the L and L+1 orbitals accommodate the doped electrons upon metal-intercalation and are well separated from the remaining low and high energy MOs. In Table I we have shown the single-particle energy gaps for phenanthrene and picene at two different values of ϵ , illustrating the separation of the FMOs from the low and high lying MOs.

TABLE I: Comparison of single-particle energy gaps (in units of t) of phenanthrene (cols 2–3) and picene (cols 4–5) for two different values of ϵ . H denote Highest Occupied MO (HOMO).

Gaps/Molecule	$ \epsilon = 0$	$ \epsilon = 0.65$	$ \epsilon = 0$	$ \epsilon = 0.65$
$\Delta_{H,L}$	1.21	1.20	1.00	0.99
$\Delta_{L,L+1}$	0.16	0.12	0.18	0.13
$\Delta_{L+1,L+2}$	0.37	0.37	0.18	0.19

Due to the tiny values of inter-molecular hoppings $t_{\mu, \nu, i, j}$ relative to $\Delta_{H,L}$ and $\Delta_{L+1,L+2}$ in phenanthrene, occupations of the lower bonding and higher antibonding MOs are not affected by band formation involving the L and L+1 orbitals only. However for picene this is not the case as $\Delta_{L,L+1} \sim \Delta_{L+1,L+2}$, and participation of the L+2 orbital can be expected. Within the reduced subspace, due to small $\Delta_{L,L+1}$, *no* Coulomb (e-e) matrix elements between L and L+1 orbitals should be ignored as well as, *all* inter-molecular hoppings between them have to be taken into consideration. The importance of the inter-molecular L-L+1 hoppings will be discussed in Sec-III. The reduced Hamiltonian $H_{L,L+1}^{PPP}$ within the subspace of the L and L+1 orbitals can be written as,

$$\begin{aligned}
H_{L,L+1}^{PPP} = & \sum_{\mu,k,\sigma} \epsilon_k N_{\mu,k,\sigma} + \sum_{\mu,k,\sigma} \tilde{U}_{k,k}^{(d),\sigma,-\sigma} N_{\mu,k,\sigma} N_{\mu,k,-\sigma} + \sum_{\mu,k \neq k',\sigma} \tilde{U}_{k,k'}^{(d),\sigma,-\sigma} N_{\mu,k,\sigma} N_{\mu,k',-\sigma} + \sum_{\mu,k \neq k',\sigma} \tilde{U}_{k,k'}^{(d),\sigma,\sigma} N_{\mu,k,\sigma} N_{\mu,k',\sigma} \\
& + \sum_{\mu,k_1 \neq k_2, k_3 \neq k_4, \sigma} \tilde{U}_{k_1,k_2}^{(o),\sigma,-\sigma} a_{\mu,k_1,\sigma}^\dagger a_{\mu,k_2,\sigma} a_{\mu,k_3,-\sigma}^\dagger a_{\mu,k_4,-\sigma} + \sum_{\mu \neq \nu, k, k', \sigma} t_{\mu,\nu}^{k,k'} a_{\mu,k,\sigma}^\dagger a_{\nu,k',\sigma}.
\end{aligned} \tag{4}$$

Here, k indices refer to L and L+1 orbitals. In the Appendix we show the derivation of $H_{L,L+1}^{PPP}$ and discuss the various terms occurring in reduced Hamiltonian.

We numerically study finite zig-zag 1D lattices [see Fig. 1] with nearest and next-nearest neighbor hoppings between the molecules, using the Diagrammatic Valence Bond (DVB) technique^{47–49}. This is an exact diagonalization method utilizing the complete, non-orthogonal, S_{total} and S_{total}^z conserving valence bond basis. Within the reduced subspace of the FMOs, the real space nearest and next-nearest neighbor hoppings translate to 3 kinds of inter-molecular inter-orbital hoppings, namely, $t_j^{L,L}$, $t_j^{L,L+1}$ and $t_j^{L+1,L+1}$; $j = 1, 2$, denote nearest and next-nearest neighbors. The parameters of our reduced Hamiltonian [Eq. 4] are $\Delta_{L,L+1}$, intra-molecular e-e interactions, i.e., U and κ , and the multiple inter-molecular hopping integrals. While the first two are obtained from molecular calculations, we parametrize the inter-

molecular hoppings based on our previous work²². The parametrized values of the inter-molecular hopping integrals (in eV) considered in this work are as follows: $t_1^{L,L} = 0.15$, $t_1^{L,L+1} = 0.05$, $t_1^{L+1,L+1} = 0.10$; $t_2^{L,L} = t_2^{L+1,L+1} = 0.075$, $t_2^{L,L+1} = 0.025$. We consider $\Delta_{L,L+1} = 0.3$ eV, $0 \leq U \leq 10$ (in eV), and $\kappa = 1.0, 3.0$. We study 1D phenanthrene lattices with 10 ions (20 MOs) with charges -1 (10 electrons) and -3 (30 electrons), and 8 ions (16 MOs) with charge -2 (16 electrons). Studying 10 ions with molecular charge -2 , i.e., 20 electrons on 20 MOs, is beyond current computational capacity. We compute the ratio of the average charge densities on the L and L+1 orbitals, i.e., $\frac{n_{L+1}}{n_L}$, and spin-spin correlation functions given by $\langle S_{1,k}^z S_{\mu,k}^z \rangle$, respectively; $k = L, L+1$ and $\mu = \text{molecule index}$. Apart from these observables, we also calculate the kinetic energies of the L and L+1 orbitals,

$$K_p = \left| \sum_{\mu,\sigma} \left(t_1^{p,p} \langle a_{\mu,p,\sigma}^\dagger a_{\mu,p,\sigma} + \text{H.C.} \rangle + t_2^{p,p} \langle a_{\mu,p,\sigma}^\dagger a_{\mu,p,\sigma} + \text{H.C.} \rangle \right) \right|. \tag{5}$$

Here, μ is the index of the molecule and $p \in [L, L+1]$; other symbols have already been defined.

III. SUMMARY OF PREVIOUS RESULTS

Previously²² we had derived an effective Hamiltonian, $H_{Hub}^{L,L+1}$ for metal-intercalated phenanthrene crystals within the localized basis of the L and L+1 orbitals of individual phenanthrene molecules. The reason for choosing these MOs have already been discussed in the previous section. The individual phenanthrene molecules were described by the Hubbard model with short range (onsite) e-e interactions. In the $U = 0$ limit, the band structure of $H_{Hub}^{L,L+1}$ was composed of MOs of predominantly either L- or L+1-character. In both our past and present study, we call these as L- and L+1-derived MOs. We found that in the *absence* of the $t_j^{L,L+1}$ terms, the band structure of $H_{Hub}^{L,L+1}$ consisted of L-derived MOs lying below the Fermi level and L+1-derived MOs above the Fermi level [see Fig. 2(a)]; the Fermi level lies between

the HOMO and the LUMO of the phenanthrene crystal with $E_F = 0$. When electrons were filled in this band structure, we found that the monoanion and the dianion crystals of phenanthrene had all L-derived MOs occupied *only*. As a result $n_{L+1}/n_L = 0$ for both, where n_L and n_{L+1} were the average orbital occupancies of the L- and L+1-derived MOs. In the trianion crystal however, electrons occupy both the L- and L+1-derived MOs, thereby making $n_{L+1}/n_L = 0.5$. In the *presence* of the $t_j^{L,L+1}$ terms however, we found that in the uncorrelated limit, both in 1D and 2D, the band structure of phenanthrene crystals consist of clusters of L- and L+1-derived MOs occurring alternately as shown in Fig. 2(b). As a result, the ratio $n_{L+1}/n_L > 0$ and 0.5 in the dianion and trianion crystals, respectively. The monoanion by virtue of its molecular charge, continued to have all L-derived MOs occupied only, thereby making $n_{L+1}/n_L = 0$. Therefore in the $U = 0$ limit, presence of the $t_j^{L,L+1}$ terms enforced charge asymmetry between the monoanion and trianion crystals. *Note that there is no charge asymmetry between molecular valences -1 and -3 in the absence*

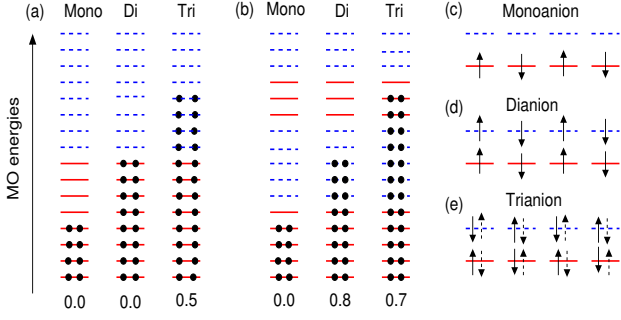


FIG. 2: (Color online) Tight-binding energy level diagram of a 1D lattice of 8 phenanthrene ions, i.e., 16 MOs, without (a) and with (b) the $t_j^{L,L+1}$ terms, illustrating the role of band-width induced charge asymmetry between the mononion and trianion crystals at $U = 0$; solid black dots indicate electrons. The numbers given below each ion in (a) and (b) indicate the ratio n_{L+1}/n_L ; n_L and n_{L+1} are the number of electrons in the MOs with L- and L+1-character, respectively. Schematic representation (c)-(e) of the normal states of the three kinds of phenanthrene ionic crystals in the presence of short range correlations; solid and broken arrows indicate 1 and 1/2 electron, respectively (see Sec-III for details). Solid (red) and broken (blue) lines indicate the L- and L+1-derived MOs, respectively.

of the $t_j^{L,L+1}$ terms and both are $\frac{1}{2}$ -filled systems. The band-width effect was further enhanced by short range e-e interactions, resulting in distinct charge-orbital orderings in the three kinds of phenanthrene ionic crystals. In the dianion crystals the L- and L+1-derived MOs became equally populated with L-L+1 intra-molecular ferromagnetic spin ordering and, L-L and L+1-L+1 intermolecular antiferromagnetic spin-spin couplings. The trianion crystal on the other hand behaved as a nearly degenerate $\frac{3}{4}$ -filled two-band system with no spin order. The monoanion however, continued to be $\frac{1}{2}$ -filled with antiferromagnetic coupling between the filled L-derived MOs.

IV. RESULTS AND DISCUSSION

In Sec-III we discussed the effect of short range e-e interactions on the normal state of metal-intercalated phenanthrenes. Here we present our results showing the effect of long range Coulomb correlations on the same. For simplicity's sake, we will be referring to the diagonal e-e repulsion terms between opposite spin electrons as $\tilde{U}_{L,L}^{\uparrow,\downarrow}$, $\tilde{U}_{L+1,L+1}^{\uparrow,\downarrow}$ and $\tilde{U}_{L,L+1}^{\uparrow,\downarrow}$. The diagonal term $\tilde{U}_{L,L}^{(d),\sigma,\sigma}$ representing e-e repulsion between same spin electrons will be denoted as $\tilde{U}_{L,L+1}^{\uparrow,\uparrow}$ while the off-diagonal component $\tilde{U}_{L,L+1}^{(o),\sigma,-\sigma}$ will be denoted as $\tilde{U}_{L,L+1}^{2e}$. In Table II we have compared the magnitudes of the various e-e interaction terms present in $H_{L,L+1}^{Hub}$ and $H_{L,L+1}^{PPP}$ at two different values of U and $\Delta_{L,L+1} = 0.3$ eV. We find that i) magnitudes of all e-e interaction terms in $H_{L,L+1}^{PPP}$ are

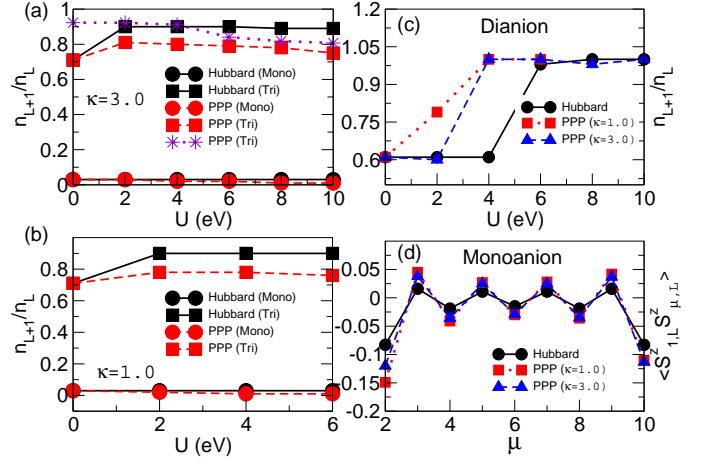


FIG. 3: (Color online) (a) and (b): Variation in $\frac{n_{L+1}}{n_L}$ with U in the models $H_{L,L+1}^{Hub}$ (black solid lines) and $H_{L,L+1}^{PPP}$ (red dashed lines), for the monoanion (circles) and trianion (squares) crystals, respectively. Violet dotted line with stars in (a) is for the trianion crystal with different set of hopping parameters (see text for details). (c): Change in $\frac{n_{L+1}}{n_L}$ as a function of U for the dianion crystal; solid black, dotted red and dashed blue curves correspond to $H_{L,L+1}^{Hub}$ model, and $H_{L,L+1}^{PPP}$ model with $\kappa = 1, 3$, respectively. (d): Spin-spin correlation functions in the monoanion for the two models at $U = 6.0$ eV; μ is the index of the molecule. L-L+1 and L+1-L+1 spin-spin correlations being zero, are not shown. In all the plots $\Delta_{L,L+1} = 0.3$ eV.

larger than those in $H_{L,L+1}^{Hub}$ due to renormalization, ii) magnitude of $\tilde{U}_{L,L+1}^{\uparrow,\downarrow}$ term in $H_{L,L+1}^{PPP}$ is either comparable to or larger than both $\tilde{U}_{L,L}^{\uparrow,\downarrow}$ and $\tilde{U}_{L+1,L+1}^{\uparrow,\downarrow}$ depending on the screening constant, and iii) the repulsion term $U_{L,L+1}^{\uparrow,\uparrow}$ is found to be comparable to $\tilde{U}_{L,L}^{\uparrow,\downarrow}$ and $\tilde{U}_{L+1,L+1}^{\uparrow,\downarrow}$ for smaller values of κ and larger values of U . We also find that when $U > 6$ eV and $\kappa = 1$, the e-e interaction parameters in $H_{PPP}^{L,L+1}$ acquire unphysical values. Consequently in Fig. 3(b) the X-axis is truncated at $U = 6.0$ eV. Based on Table II we now explain the behavior of the normal states of the three kinds of phenanthrene ionic crystals in the presence of long range e-e correlations.

TABLE II: Comparison of the magnitudes of various e-e interaction terms in $H_{L,L+1}^{Hub}$ and $H_{L,L+1}^{PPP}$ for $\kappa = 1, 3$, at $U = 4.0$ eV (columns 2-4) and 8.0 eV (columns 5-7) and $\Delta_{L,L+1} = 0.3$ eV.

Param	$H_{L,L+1}^{Hub}$	$\kappa = 1$	$\kappa = 3$	$H_{L,L+1}^{Hub}$	$\kappa = 1$	$\kappa = 3$
$\tilde{U}_{L,L}^{\uparrow,\downarrow}$	0.443	0.789	0.558	0.886	1.579	1.117
$\tilde{U}_{L+1,L+1}^{\uparrow,\downarrow}$	0.429	0.787	0.548	0.859	1.573	1.098
$\tilde{U}_{L,L+1}^{\uparrow,\downarrow}$	0.161	0.935	0.419	0.322	1.869	0.838
$\tilde{U}_{L,L+1}^{\uparrow,\uparrow}$	0.000	0.774	0.258	0.000	1.547	0.516
$\tilde{U}_{L,L+1}^{2e}$	0.161	0.134	0.152	0.322	0.267	0.304

As seen from Figs. 3(a) and (b), the ratio n_{L+1}/n_L in

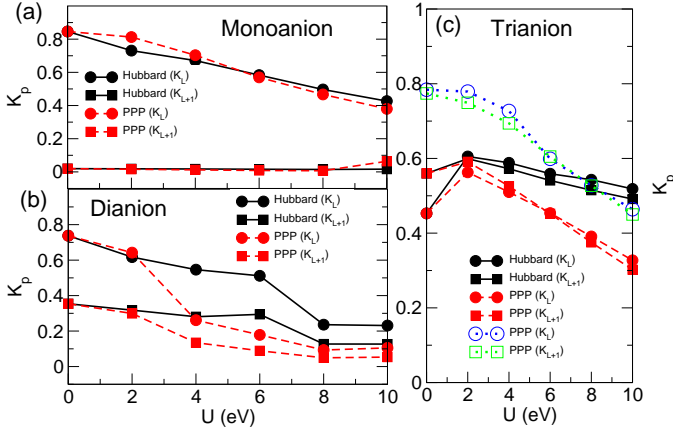


FIG. 4: (Color online) Change in K_L (circles) and K_{L+1} (squares) with U for the monoanion (a), dianion (b) and trianion (c) crystals. Solid (dashed) black (red) curves pertain to $H_{L,L+1}^{Hub}$ ($H_{L,L+1}^{PPP}$) model. In all the plots $\Delta_{L,L+1} = 0.3$ eV and $\kappa = 3.0$. In (c), the dotted blue and green lines with open circles and squares, respectively, are for a different set of inter-molecular hoppings (see text for details).

the monoanion crystal is 0, indicating that the populations of the L- and L+1-derived MOs are respectively, $\dots 1111 \dots$ and $\dots 0000 \dots$; 1 and 0 refer to singly occupied and empty sites, respectively. Thus with long range interactions also, the electrons in the monoanion crystal are "confined" to the L-derived orbitals only. We therefore expect, as we had observed for $H_{L,L+1}^{Hub}$, that the electrons will be antiferromagnetically coupled to each other as this is the most stable configuration. Plot of inter-molecular L-L spin-spin correlations at $U = 6.0$ eV and $\Delta_{L,L+1} = 0.3$ eV confirms our expectation and indicate antiferromagnetic (AFM) spin ordering in the monoanion [Fig. 3(d)]. The antiferromagnetic interactions between the L-derived MOs are however stronger than that found with short range correlations, indicating that long range correlations stabilize the $\frac{1}{2}$ -filled AFM state more than short range interactions. This is because of increased magnitude of the $U_{L,L}^{\uparrow\downarrow}$ term due to renormalization [see Table II]. Note that smaller values of the screening constant κ sustains larger AFM couplings because the intra-molecular Coulomb potential $V_{i,j}$ becomes "steeper" with decrease in κ . As the L-derived orbitals are occupied only, K_L is non-zero as seen from Fig. 4(a). Due to electron hoppings, the site charge densities of the L-derived orbitals changes from $\dots 1111 \dots$ to $\dots 1201 \dots$ to $\dots 1210 \dots$; here, 2 refers to doubly occupied sites. The tendency to form 2s and 0s will decrease with increase in U , which dictates all the e-e repulsion terms in $H_{L,L+1}^{PPP}$. Therefore in Fig. 4(a) we find that with increase in U , K_L decreases nearly monotonically. Thus, from Figs. 3(a), (b) and (d), and Fig. 4(a) we find that the behavior of the monoanion crystal is the same with both short and long range e-e interactions. We therefore surmise that long range correlations do not affect the nor-

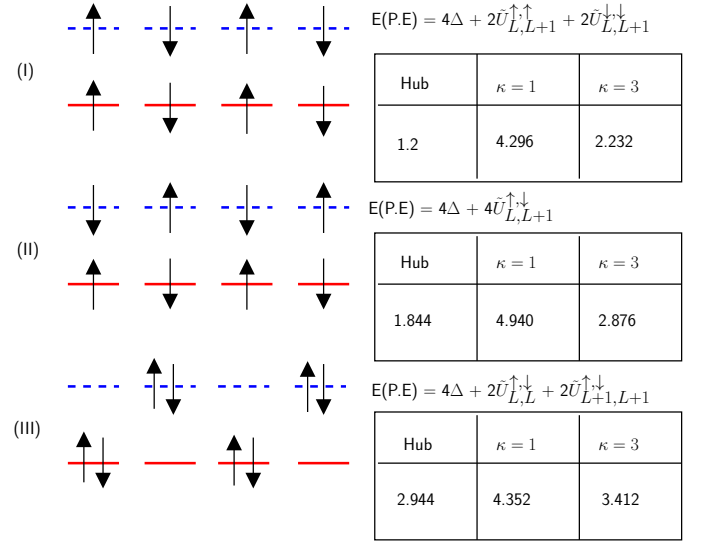


FIG. 5: (Color online) Schematic depiction of three configurations of the dianion crystal with equally populated L- (solid red line) and L+1-derived (dashed blue line) orbitals. The analytical expression of the potential energy, $E(P.E)$, of each configuration is indicated along with its numerical value in the table underneath, for $H_{L,L+1}^{Hub}$ and $H_{L,L+1}^{PPP}$ ($\kappa = 1, 3$). Arrows denote electrons, $U = 4.0$ eV, and $\Delta = \Delta_{L,L+1} = 0.3$ eV. The numerical values of $E(P.E)$ are obtained using the analytical expression and Table II

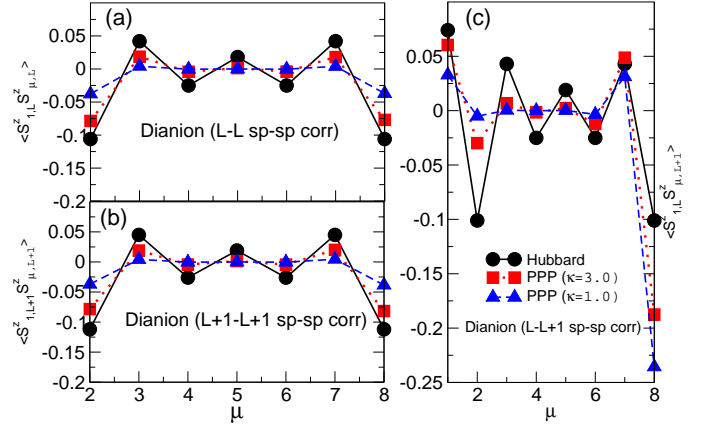


FIG. 6: (Color online) Spin-spin correlations for the dianion crystal in the $H_{L,L+1}^{Hub}$ model (solid black line with circles) and the $H_{L,L+1}^{PPP}$ model with $\kappa = 1$ (dotted red line with squares) and $\kappa = 3$ (dashed blue line with triangles), respectively. (a), (b) and (c) show the plots of $\langle S_{1,L}^z S_{\mu,L}^z \rangle$, $\langle S_{1,L+1}^z S_{\mu,L+1}^z \rangle$, and $\langle S_{1,L}^z S_{\mu,L+1}^z \rangle$, respectively, for $\Delta_{L,L+1} = 0.3$ eV and $U = 6.0$ eV; μ is the index of the molecule.

mal state of the monoanion crystal and it continues to behave as a $\frac{1}{2}$ -filled Mott-Hubbard semiconductor.

We have already seen in Sec-III that the band structure of the dianion crystal is such that it allows electron exchange between the L- and L+1-derived MOs at $U = 0$. Population exchange between these MOs is further enhanced by short range e-e interactions²² result-

ing in $n_{L+1}/n_L \rightarrow 1$. From Fig. 3(c) it is observed that with long range correlations also, as U is increased, $n_{L+1}/n_L \rightarrow 1$. However, compared to short range interactions, long range correlations bring about population equalization “faster”, i.e., at relatively smaller U values. Furthermore, the atomic U at which n_{L+1} becomes equal to n_L is dictated by the screening constant, i.e., the “steepness” of the intra-molecular potential $V_{i,j}$. $n_{L+1}/n_L \rightarrow 1$ in the dianion crystals in the presence of long range correlations is very intriguing because the repulsion term $\tilde{U}_{L,L+1}^{\uparrow\uparrow}$ is supposed to hinder population equalization. To understand this behavior of dianion crystals, we compare the potential energies, $E(P.E)$, of three configurations with equally populated L- and L+1-derived MOs in Fig. 5. We choose these because configurations with equally populated L- and L+1-derived orbitals have maximum kinetic stability and are thus prone to be favored over other configurations. From Fig. 5 it is evinced that configurations like (I) have the minimum potential energy and are hence dominant in the ground state of the dianion crystal. This explains the behavior of the spin-spin correlation functions shown in Fig. 6: While the inter-molecular L-L and L+1-L+1 spin-spin correlations are antiferromagnetic in nature, the intra-molecular L-L+1 spin-spin couplings are ferromagnetic. Depending on the magnitude of U the dianion crystal behaves as a two-band system with either $0 < n_{L+1}/n_L < 1$ or $n_{L+1}/n_L = 1$. These two ground states being different from each other, are expected to have different kinetic energies. This is indeed the case as seen from Fig. 4(b). If we compare Figs. 3(c) and 4(b) it is found that the U value at which n_{L+1}/n_L increases suddenly coincides with the U value at which K_L and K_{L+1} show sudden decrease. Once population equalization has occurred, $K_L \simeq K_{L+1}$ and both of them decrease monotonically with U as the L- and L+1-derived orbitals become effectively $\frac{1}{2}$ -filled. Due to finite size effect the values of K_L and K_{L+1} are not of same magnitudes although in the thermodynamic limit they are expected to be same.

By virtue of the band-width effect, crystals of phenanthrene trianions have $n_{L+1}/n_L > 0.5$ at $U = 0$. From Figs. 3(a) and (b) it is observed that short range e-e interactions further enhance this charge transfer between the L- and L+1-derived orbitals, thereby making $n_{L+1}/n_L \rightarrow 1.0$. Long range correlations on the other hand suppress this tendency and coerce n_{L+1}/n_L to approach its $U = 0$ value with increase in U , as evinced from the same figures. In other words, the tendency of trianion crystals to form a nearly-degenerate $\frac{3}{4}$ -filled system is hindered by long range correlations. In order to understand this, we will first briefly discuss how short range e-e interactions drive trianion crystals toward population equalization. Consider the Mott-Hubbard configuration [configuration (I) in Fig. 7]. Although it has the minimum potential energy compared to all other configurations, its kinetic stability is also minimum. This is because of K_L being zero. Any other configuration with $n_{L+1}/n_L > 0.5$ has more kinetic stability due to contribution from both K_L and

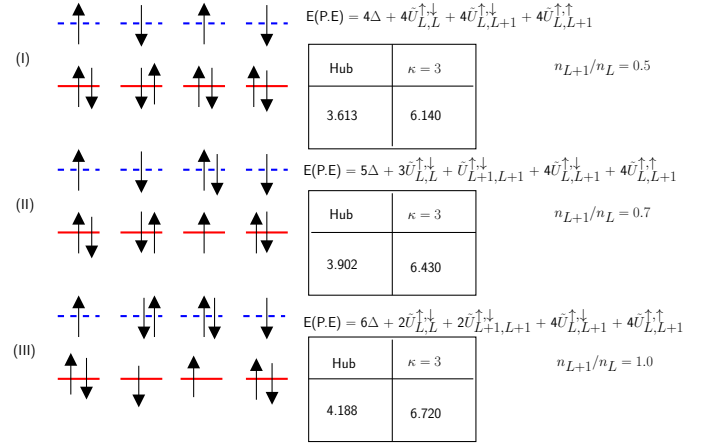


FIG. 7: (Color online) Schematic representation of three configurations of the trianion crystal along with their corresponding potential energies, $E(P.E)$. The table for each configuration depict the numerical values of $E(P.E)$ for $H_{L,L+1}^{Hub}$ and $H_{L,L+1}^{PPP}$ ($\kappa = 1, 3$), respectively, at $U = 4$ eV; these values have been obtained using the analytical expressions of $E(P.E)$ and Table II. Solid red and dashed blue lines depict the L- and L+1-derived MOs, respectively; \uparrow (\downarrow) denote spin-up (spin-down) electrons. The ratio n_{L+1}/n_L for each configuration is also shown. (I) is the Mott-Hubbard configuration, (II) is the $U = 0$ configuration, and (III) is the $\frac{3}{4}$ -filled two-band system.

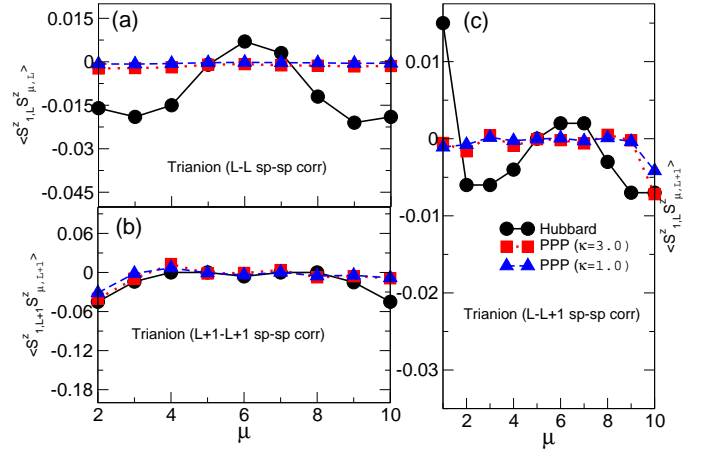


FIG. 8: (Color online) Change in $\langle S_{1,L}^z S_{\mu,L}^z \rangle$ (a), $\langle S_{1,L+1}^z S_{\mu,L+1}^z \rangle$ (b) and $\langle S_{1,L}^z S_{\mu,L+1}^z \rangle$ (c), with U of the trianion crystal at $\Delta_{L,L+1} = 0.3$ eV and $U = 6.0$ eV; μ is the molecule index. Solid black lines with circles indicate the $H_{L,L+1}^{Hub}$ model while dotted (dashed) red (blue) curves with squares (triangles) refer to $H_{L,L+1}^{PPP}$ with $\kappa = 1$ ($\kappa = 3$), respectively.

K_{L+1} . This gain in kinetic energy overrides the increase in potential energy due to electron exchange between the L- and L+1-derived orbitals. Now, consider configurations (II) and (III) of Fig. 7; while (II) has $n_L > n_{L+1}$, (III) has $n_L = n_{L+1}$. Although the potential energies of these configurations are comparable, any *double occu-*

pancy conserving electron hops for configuration (II) will lead to an increase in potential energy. No potential energy increase will however occur for configuration (III) by virtue of these *double occupancy conserving* hops; we define *double occupancy conserving* hoppings as electron hops within the L-derived (L+1-derived) orbitals such that the number of doubly occupied L-derived (L+1-derived) orbitals remain unchanged²². In other words, configurations with $n_{L+1}/n_L \simeq 1$ will have higher kinetic stability and therefore dominate in the ground state wavefunction at $U > 0$.

With long range correlations however, configurations like (II) dominate the ground state wavefunction and therefore n_{L+1}/n_L (at $U > 0$) \rightarrow n_{L+1}/n_L (at $U = 0$). This implies that the *double occupancy conserving* electron hops fail to provide configurations like (III) the kinetic stability needed to overcome the initial potential energy gain. If we look at the magnitudes of $E(P.E)$ in Fig. 7, we find that magnitudes of the potential energies of the configurations in the presence of long range correlations are almost double compared to their magnitudes with short range correlations. This indicates that the behavior of the trianion crystals with long range e-e interactions will be dominated by $E(P.E)$ rather than kinetic stability. Simply stated, this implies that with increase in U the ground state wave function of the trianion crystal will be dominated by configurations which are kinetically more stable than the Mott-Hubbard configuration but with the minimum number of electrons promoted from the L- to the L+1-derived orbitals. For example, in the lattice of 20 MOs with 30 electrons, for $0 < U \leq 10$, only 2 electrons are transferred from the L- to the L+1-derived MOs, thereby making $n_{L+1}/n_L \sim 0.7$ [see Figs. 3(a) and (b)]. We believe that the behavior of the trianion crystal in the presence of long range correlations is due to smaller band-width compared to the e-e interactions. In case of short range correlations the band-width was comparable to the e-e interactions and thus allowed cooperation between the two. There are two possible ways to increase the band-width: (a) Increase the magnitudes (within realistic limits) of the inter-molecular inter-orbital hopping terms, i.e., $t_j^{\mu,\nu}$, and, (b) increase the lattice sizes chosen. However, (b) is not possible in the present context as the lattices used are the largest possible within our exact diagonalization study. Therefore if the behavior of the trianion crystal does not change upon increasing the magnitudes of the $t_j^{\mu,\nu}$ terms, then small system size is the reason for the trianion crystal for behaving differently in the presence of long range correlations.

We computed n_{L+1}/n_L and K_L and K_{L+1} for the trianion crystal with larger hopping parameters, i.e., larger band-width, at $\Delta_{L,L+1} = 0.3$ eV and $\kappa = 3.0$; $t_1^{L,L} = 0.175$, $t_1^{L,L+1} = 0.075$, $t_1^{L+1,L+1} = 0.125$, and, $t_2^{L,L} = t_2^{L+1,L+1} = 0.1$, $t_2^{L,L+1} = 0.05$; all hopping terms are realistic and expressed in eV. The plots of n_{L+1}/n_L and the kinetic energies versus U with the new $t_j^{k,k'}$ terms are shown in Figs. 3(a) and 4(c), respectively. We find

that the behavior of the trianion crystal at large U remains unchanged even with increased hopping parameters. We therefore conclude that long range interactions demand longer system sizes compared to those studied in the present work. The L-L, L+1-L+1 and L-L+1 spin-spin correlations [Figs. 8(a)-(c)] however show that there is no spin ordering in the trianion as was found with short range correlations. This again indicates that the ground state of the trianion is not of the Mott-Hubbard type with $n_L = 2$ and $n_{L+1} = 1$, but with n_L and n_{L+1} slightly less and more than 2 and 1, respectively.

V. CONCLUSIONS AND DISCUSSIONS

In this work we have addressed the effect of long range Coulomb correlations on the normal state of metal-intercalated phenacene crystals, taking phenanthrene as example. The individual phenacene molecules have been modeled by the Pariser-Parr-Pople Hamiltonian. We derive an effective correlated model Hamiltonian $H_{L,L+1}^{PPP}$ to describe the phenacene ions in the solid state within a localized basis of the L and L+1 FMOs. We find that long range correlations not only renormalize the Coulomb terms occurring in $H_{L,L+1}^{H_{ub}}$ but also introduce an additional intra-molecular repulsion term between same spin electrons; $H_{L,L+1}^{H_{ub}}$ is the effective Hamiltonian obtained by describing the individual phenacene molecules by the Hubbard model with short range e-e interactions. It is found that the normal states of the monoanion and dianion molecular solids remain unaffected by the presence of long range interactions. The monoanion crystal continues to behave as a single-band $\frac{1}{2}$ -filled Mott-Hubbard semiconductor with L-L antiferromagnetic spin order. The dianion crystal undergo population equalization with increase in the strength of e-e repulsion, i.e., U . Spin-spin correlations show that the inter-molecular L-L and L+1-L+1 spin couplings are antiferromagnetic while the intra-molecular L-L+1 spin couplings are ferromagnetic. The trianion's behavior with short and long range interactions is however different. With short range correlations the trianion is a nearly $\frac{3}{4}$ -filled two-band system without any spin order. However, in the presence of long range interactions, with increase in U , the tendency towards population equalization between the L- and L+1-derived MOs is suppressed and the ratio n_{L+1}/n_L reaches its $U = 0$ magnitude. This occurs because the system sizes chosen in this study are not large enough to provide the kinetic stability necessary for $n_{L+1}/n_L \simeq 1$. Thus the trianion crystal behaves as a two-band system with n_L slightly less than 2 and n_{L+1} slightly greater than 1, and without any spin order. We believe that larger system sizes will allow population equalization in the trianion crystal even with long range correlations. We thus conclude that the behavior of the normal state of metal-intercalated phenanthrene crystals are not affected by long range Coulomb correlations.

Occurance of SC under pressure and at a fixed carrier

concentration is a signature of C-based superconductors. While SC occurs at carrier density $\rho = 0.5$ in the CTS, both fullerides and metal-intercalated phenacenes show SC at the molecular stoichiometry of -3 . The CTS can be either electron or hole doped with one electron or hole per dimer resulting in $\rho = 0.5$. Examples of hole and electron doped CTS are κ -(BEDT) $_2$ X, where X = Cl, Br, I, (NCS) $_2$, Cu $_2$ (CN) $_3$, and, Z[Pd(dmit) $_2$] $_2$ salts, Z = P, As, Sb, respectively; here, BEDT = bisethylenedithio-tetrathiafulvalene and dmit = 1,3-dithiol-2-thione-4,5-dithiolate. In metal-intercalated phenacenes, two MOs per molecule accommodate 3 electrons and thus $\rho = \frac{3}{2}$. Similar scenario is expected in the case of doped fullerides also: 3 electrons on two non-degenerate MOs separated by a gap equal to the Jahn-Teller distortion energy, thereby giving $\rho = \frac{3}{2}$. However as discussed in Sec-I, all available theoretical works on the fullerides are based on the idea that SC occurs from an effectively $\frac{1}{2}$ -filled ($\rho = 1$) Mott-Hubbard AFM; this theoretical approach however suffers from some drawbacks, for example, it is unable to explain the absence of SC in singly-doped fullerides. Thus, it is important to revisit the mechanism of SC in doped fullerides. Also, instead of focussing on each of these three classes of C-based superconducting materials separately, stress should be given on understanding whether these materials indeed have a common normal state and thus, a common mechanism of SC.

Acknowledgement This work was supported by the U.S. Department of Energy, Office of Science, Basic Energy Sciences, under Award No. DE-FG02-06ER46315. This research used resources of the NERSC, which is supported by the Office of Science of the U.S. Department of Energy under Contract No. DE-AC02-05CH11231.

Appendix A: Derivation of the reduced Hamiltonian

The complete Hamiltonian of metal-intercalated phenacenes in the solid state, within the $2p_z$ atomic orbital basis, can be expressed as, $H = H_{intra} + H_{inter}$; H_{intra} [Eq. 1] can be broken into H_{intra}^{1e} and H_{intra}^{ee} which are the one- and many-electron components, respectively. In order to transform H from the atomic orbital basis to the MO basis, we first solve H_{intra}^{1e} exactly,

$$H_{intra}^{1e} = \sum_{\mu,k,\sigma} E_{\mu,k} a_{\mu,k,\sigma}^\dagger a_{\mu,k,\sigma}, \quad (A1)$$

where $a_{\mu,k,\sigma}^\dagger = \sum_i \psi_{\mu,k,i} c_{\mu,i,\sigma}^\dagger$ represents the k th MO of the μ -th molecule. We then express H_{intra}^{ee} and H_{inter}^{1e} within these *localized* MOs $a_{\mu,k,\sigma}^\dagger$ ^{22,50}.

$$H_{intra}^{ee}(\text{onsite}) = U \left[\sum_{\mu,k,k',i} |\chi_{\mu,i,k}|^2 |\chi_{\mu,i,k'}|^2 N_{\mu,k,\uparrow} N_{\mu,k',\downarrow} + \sum_{\mu,k_1 \neq k_2, k_3 \neq k_4, i} \left(\prod_{l=1}^4 \chi_{\mu,i,k_l} \right) a_{\mu,k_1,\uparrow}^\dagger a_{\mu,k_2,\uparrow} a_{\mu,k_3,\downarrow}^\dagger a_{\mu,k_4,\downarrow} \right] \quad (A2)$$

$$\begin{aligned} H_{intra}^{ee}(\text{long range}) = & \frac{1}{2} \left[\sum_{\mu,k,\sigma,i \neq j} V_{i,j} |\chi_{\mu,i,k}|^2 |\chi_{\mu,j,k}|^2 N_{\mu,k,\sigma} + \sum_{\mu,k,k',\sigma,i \neq j} V_{i,j} |\chi_{\mu,i,k}|^2 |\chi_{\mu,j,k'}|^2 N_{\mu,k,\sigma} N_{\mu,k',-\sigma} \right. \\ & + \sum_{\mu,k \neq k', \sigma, i \neq j} V_{i,j} |\chi_{\mu,i,k}|^2 |\chi_{\mu,j,k'}|^2 N_{\mu,k,\sigma} N_{\mu,k',\sigma} + \sum_{\mu,k_1 \neq k_2, k_3 \neq k_4; i \neq j} V_{i,j} \left\{ \prod_{l=1}^2 \chi_{\mu,i,k_l} \chi_{\mu,j,k_l} \right\} a_{\mu,k_1,\uparrow}^\dagger a_{\mu,k_2,\uparrow} a_{\mu,k_3,\downarrow}^\dagger a_{\mu,k_4,\downarrow} \\ & \left. + \sum_{\mu,k \neq k', i \neq j, \sigma} \left\{ |\chi_{\mu,i,k}|^2 \chi_{\mu,j,k} \chi_{\mu,j,k'} + |\chi_{\mu,j,k}|^2 \chi_{\mu,i,k} \chi_{\mu,i,k'} \right\} N_{\mu,k,\sigma} (a_{\mu,k,\sigma}^\dagger a_{\mu,k',\sigma} + \text{H.C.}) \right] \quad (A3) \end{aligned}$$

$$H_{inter}^{1e} = \sum_{k_1, k_2, \sigma; i \in \mu, j \in \nu, \mu \neq \nu} \chi_{\mu,i,k_1} \chi_{\nu,j,k_2} t_{\mu,\nu,i,j} a_{\mu,k_1,\sigma}^\dagger a_{\nu,k_2,\sigma} \quad (A4)$$

The matrices χ and ψ are inverses of each other and $N_{\mu,k,\sigma} = a_{\mu,k,\sigma}^\dagger a_{\mu,k,\sigma}$. The above transformation from the complete basis of atomic orbitals to the complete MO basis is *exact*. The terms $H_{intra}^{ee}(\text{onsite})$ and $H_{intra}^{ee}(\text{long range})$ correspond to the intra-molecular inter-atomic e-e repulsions due to the short and long range compo-

nents of the PPP Hamiltonian (Eq. 1). The second and fourth terms of Eq. A3 are same as the first and second terms in Eq. A2, respectively, except with different coefficients. Thus, the long range component of the PPP Hamiltonian renormalize the onsite (U -dependent) terms in Eq. A2. The third term in Eq. A3 denotes

the e-e repulsion between *parallel* spins on different MOs, *within the same molecule*; the last term in Eq. A3 depict density-dependent intra-molecular hoppings between different MOs. Eqs. A2 – A4 represent H in the complete

MO basis. The reduced Hamiltonian $H_{L,L+1}$ can be obtained by restricting the sums over the k 's in Eqs. A2 – A4 to the L and L+1 orbitals.

$$\begin{aligned}
 H_{L,L+1}^{PPP} = & \sum_{\mu,k,\sigma} \epsilon_k N_{\mu,k,\sigma} + \sum_{\mu,k,\sigma} \tilde{U}_{k,k}^{(d),\sigma,-\sigma} N_{\mu,k,\sigma} N_{\mu,k,-\sigma} + \sum_{\mu,k \neq k',\sigma} \tilde{U}_{k,k'}^{(d),\sigma,-\sigma} N_{\mu,k,\sigma} N_{\mu,k',-\sigma} + \sum_{\mu,k \neq k',\sigma} \tilde{U}_{k,k'}^{(d),\sigma,\sigma} N_{\mu,k,\sigma} N_{\mu,k',\sigma} \\
 & + \sum_{\mu,k_1 \neq k_2, k_3 \neq k_4, \sigma} \tilde{U}_{k_1,k_2}^{(o),\sigma,-\sigma} a_{\mu,k_1,\sigma}^\dagger a_{\mu,k_2,\sigma} a_{\mu,k_3,-\sigma}^\dagger a_{\mu,k_4,-\sigma} + \sum_{\mu \neq \nu, k, k', \sigma} t_{\mu,\nu}^{k,k'} a_{\mu,k,\sigma}^\dagger a_{\nu,k',\sigma}
 \end{aligned} \tag{A5}$$

In Eq. A5 all k indices denote L and L+1 MOs and $t_{\mu,\nu}^{L,L+1} = \sum_{i,j} \chi_{\mu,i,k_1} \chi_{\nu,j,k_2} t_{\mu,\nu,i,j}$. The orbital (site) energies

ϵ_k and the various spin-dependent Coulomb terms are defined as given below.

$$\begin{aligned}
 \epsilon_L &= E_L + \frac{1}{2} \sum_{i \neq j} V_{i,j} |\chi_{\mu,i,L}|^2 |\chi_{\mu,j,L}|^2; \epsilon_{L+1} = E_{L+1} + \frac{1}{2} \sum_{i \neq j} V_{i,j} |\chi_{\mu,i,L+1}|^2 |\chi_{\mu,j,L+1}|^2 \\
 \tilde{U}_{L,L}^{(d),\sigma,-\sigma} &= \sum_i |\chi_{\mu,i,L}|^2 \left(U |\chi_{\mu,i,L}|^2 + \frac{1}{2} \sum_{j \neq i} V_{i,j} |\chi_{\mu,j,L}|^2 \right); \tilde{U}_{L+1,L+1}^{(d),\sigma,-\sigma} = \sum_i |\chi_{\mu,i,L+1}|^2 \left(U |\chi_{\mu,i,L+1}|^2 + \frac{1}{2} \sum_{j \neq i} V_{i,j} |\chi_{\mu,j,L+1}|^2 \right) \\
 \tilde{U}_{L,L+1}^{(d),\sigma,-\sigma} &= \sum_i |\chi_{\mu,i,L}|^2 \left(U |\chi_{\mu,i,L+1}|^2 + \frac{1}{2} \sum_{j \neq i} V_{i,j} |\chi_{\mu,j,L+1}|^2 \right); \tilde{U}_{L,L+1}^{(d),\sigma,\sigma} = \frac{1}{2} \sum_{i,j \neq i} V_{i,j} |\chi_{\mu,i,L}|^2 |\chi_{\mu,j,L+1}|^2 \\
 \tilde{U}_{L,L+1}^{(o),\sigma,-\sigma} &= U \sum_i \chi_{\mu,i,L}^2 \chi_{\mu,i,L+1}^2 + \frac{1}{2} \sum_{i,j; j \neq i} V_{i,j} \chi_{\mu,i,L}^2 \chi_{\mu,j,L+1}^2
 \end{aligned}$$

The diagonal Coloumb terms, $U_{k,k}^{(d),\sigma,-\sigma}$ $k \in [L, L+1]$, denote the intra-molecular Coulomb repulsions between two electrons of opposite spins occupying orbital k . When both the L and L+1 orbitals on the *same* molecule are singly occupied by electrons with *opposite* (*same*) spins, the e-e repulsion is denoted by $U_{L,L+1}^{(d),\sigma,-\sigma}$ ($U_{L,L+1}^{(d),\sigma,\sigma}$). Apart from the four diagonal Coulomb terms, two off-diagonal terms of equal magnitude and denoted by $U_{L,L}^{(o),\sigma,-\sigma}$ are also present in Eq. A5. One of them is referred to as the two-electron (2e) hopping term and is responsible for promoting an electron pair from the L orbital to the L+1 orbital and vice versa. The other off-diagonal term gives rise to Hund's coupling between the singly-occupied L and L+1 orbitals on the same molecule²². The magnitudes of $U_{L,L+1}^{(d),\sigma,-\sigma}$ and $U_{L,L+1}^{(o),\sigma,-\sigma}$ are equal in the absence of long range e-e interactions.

However, in the presence long range e-e interactions it is found that $|U_{L,L+1}^{(d),\sigma,-\sigma}| > |U_{L,L+1}^{(o),\sigma,-\sigma}|$ and occurs due to $\sum_{i,j; j \neq i} V_{i,j} \chi_{\mu,i,L}^2 \chi_{\mu,j,L+1}^2$ being negative. Although the energies of the L and L+1 orbitals, namely, E_L and E_{L+1} , get renormalized, $\Delta_{L,L+1}$ does not change. Note that in Eq. A5 the density-dependent hopping term (last term in Eq. A3) is absent. This is because density-dependent hoppings are important only when orbitals of same symmetry are involved. Thus for phenanthrene with FMOs of different symmetries, this term does not contribute. However, for phenacenes like picene, where each molecule can behave as a three-orbital system due to $\Delta_{L,L+1} = \Delta_{L+1,L+2}$, this term is expected to have a non-zero contribution; $\Delta_{L+1,L+2}$ is the single-particle gap between the LUMO+1 LUMO+2 levels.

¹ Y. Tokura and N. Nagaosa, Science **288**, 462 (2000).

² M. Imada, A. Fujimori, and Y. Tokura, Rev. Mod. Phys. **70**, 1039 (1998).

³ A. P. Mackenzie and Y. Maeno, Rev. Mod. Phys. **75**, 657

- (2003).
- ⁴ S. Nakatsuji and Y. Maeno, Phys. Rev. Lett. **84**, 2666 (2000).
 - ⁵ G. Khaliullin and S. Maekawa, Phys. Rev. Lett. **85**, 3950 (2000).
 - ⁶ G. Khaliullin, P. Horsch, and A. M. Oles, Phys. Rev. Lett. **86**, 3879 (2001).
 - ⁷ S. Ishihara, T. Hatakeyama, and S. Maekawa, Phys. Rev. B **65**, 64442 (2002).
 - ⁸ Y. Maeno, H. Hashimoto, K. Yoshida, S. Nishizaki, T. Fujita, J. G. Bednorz, and F. Lichtenberg, Nature **372**, 532 (1994).
 - ⁹ T. Ishiguro, K. Yamaji, and G. Saito, Organic Superconductors (Springer-Verlag, New York, 1998).
 - ¹⁰ O. Gunnarsson, Rev. Mod. Phys. **69**, 575 (1997).
 - ¹¹ Y. Iwasa and T. Takenobu, J. Phys.: Condens. Matter **15**, R495 (2003).
 - ¹² M. Capone, M. Fabrizio, C. Castellani, and E. Tosatti, Rev. Mod. Phys. **81**, 943 (2009).
 - ¹³ R. Mitsuhashi et al., Nature **464**, 76 (2010).
 - ¹⁴ Y. Kubozono et al., Phys. Chem. Chem. Phys. **13**, 16476 (2011).
 - ¹⁵ X. Wang et al., Nature Communications **2**, 507 (2011).
 - ¹⁶ X. F. Wang et al., Phys. Rev. B **84**, 214523 (2011).
 - ¹⁷ X. F. Wang et al., J. Phys.: Condens. Matter **24**, 345701 (2012).
 - ¹⁸ G. A. Artioli and L. Malavasi, J. Mater. Chem. C **2**, 1577 (2014).
 - ¹⁹ M. Yano, M. Endo, Y. Hasegawa, R. Okada, Y. Yamada, and M. Sasaki, J. Chem. Phys. **141**, 034708 (2014).
 - ²⁰ J. Merino and R. H. McKenzie, Phys. Rev. Lett. **87**, 237002 (2001).
 - ²¹ R. T. Clay, S. Dayal, H. Li, and S. Mazumdar, Phys. Stat. Solidi **249**, 991 (2012).
 - ²² T. Dutta and S. Mazumdar, Phys. Rev. B **89**, 245129 (2014).
 - ²³ G. A. Artioli, F. Hammerath, M. C. Mozzati, P. Carretta, F. Corana, B. Mannucci, S. Margadonnad, and L. Malavasi, Chem. Commun. **51**, 1092 (2015).
 - ²⁴ A. Y. Ganin et al., Nature Materials **7**, 367 (2008).
 - ²⁵ A. Y. Ganin et al., Nature **466**, 221 (2010).
 - ²⁶ Y. Takabayashi et al., Science **323**, 1585 (2009).
 - ²⁷ M. Capone, M. Fabrizio, C. Castellani, and E. Tosatti, Science **296**, 2364 (2002).
 - ²⁸ Y. Nomura, S. Sakai, M. Capone, and R. Arita, J. Phys.: Condens. Matter (Topical Reviews) **28**, 153001 (2016).
 - ²⁹ J. Schmalian, Phys. Rev. Lett. **81**, 4232 (1998).
 - ³⁰ M. Vojta and E. Dagotto, Phys. Rev. B **59**, R713 (1999).
 - ³¹ B. Kyung and A. M. S. Tremblay, Phys. Rev. Lett. **97**, 046402 (2006).
 - ³² B. J. Powell and R. H. McKenzie, Phys. Rev. Lett. **94**, 047004 (2005).
 - ³³ B. J. Powell and R. H. McKenzie, Phys. Rev. Lett. **98**, 027005 (2007).
 - ³⁴ R. T. Clay, H. Li, and S. Mazumdar, Phys. Rev. Lett. **101**, 166403 (2008).
 - ³⁵ S. Dayal, R. T. Clay, and S. Mazumdar, Phys. Rev. B **85**, 165141 (2012).
 - ³⁶ L. F. Tocchio, A. Parola, C. Gros, and F. Becca, Phys. Rev. B **80**, 064419 (2009).
 - ³⁷ T. Watanabe, H. Yokoyama, Y. Tanaka, and J. Inoue, Phys. Rev. B **77**, 214505 (2008).
 - ³⁸ N. Gomes, R. T. Clay, and S. Mazumdar, J. Phys. Condens. Matter **25**, 385603 (2013).
 - ³⁹ T. Yanagisawa, New J. Phys. **15**, 033012 (2013).
 - ⁴⁰ M. F. Craciun et al., Phys. Rev. B **79**, 125116 (2009).
 - ⁴¹ R. Pariser and R. G. Parr, J. Chem. Phys. **21**, 466 (1953).
 - ⁴² J. A. Pople, Trans. Farad. Soc. **49**, 1375 (1953).
 - ⁴³ F. P. A. Fabbiani, D. R. Allan, S. Parsons, and C. R. Pulham, Acta Cryst. **B62**, 826 (2006).
 - ⁴⁴ Z. Huang, C. Zhang, and H.-Q. Lin, Scientific Reports **2**, 922 (2012).
 - ⁴⁵ M. Chandross, S. Mazumdar, M. Liess, P. A. Lane, Z. V. Vardeny, M. Hamaguchi, and K. Yoshino, Phys. Rev. B **55**, 1486 (1997).
 - ⁴⁶ K. Ohno, Theor. Chim. Acta **55**, 1486 (1997).
 - ⁴⁷ Z. G. Soos and S. Ramasesha, Phys. Rev. B **29**, 5410 (1984).
 - ⁴⁸ S. Ramasesha and Z. G. Soos, Int. J. Quant. Chem. **XXV**, 1003 (1984).
 - ⁴⁹ S. Ramasesha, Chem. Phys. Lett. **130**, 522 (1986).
 - ⁵⁰ M. Chandross, Y. Shimoi, and S. Mazumdar, Phys. Rev. B **59**, 4822 (1999).